Optimal Flight Paths Through Microburst Wind Profiles

Mark L. Psiaki* and Robert F. Stengel†
Princeton University, Princeton, New Jersey

The problem of safe microburst wind shear encounter during the approach and climb-out flight phases is addressed using flight path optimization. The purpose is to investigate the physical limits of safe penetration and to determine control strategies that take full advantage of those limits. Optimal trajectories for both jet transport and general aviation aircraft were computed for encounters with idealized and actual microburst profiles. The results demonstrate that limits on control system design rather than on the aircraft's physical performance may be the deciding factor in an aircraft's capability for safe passage through a wide class of microbursts. The best control strategies involved responding to airspeed loss in an unconventional manner by raising the nose to maintain lift.

Nomenclature

$\bar{c}$ = mean aerodynamic chord
C_D = drag coefficient
C_L = lift coefficient
C_M = pitching moment coefficient
$E(\ )$ = propeller efficiency factor
$f(\ )$ = right-hand side of a system of differential equations
$\hat{f}(\ )$ = right-hand side of a system of difference equations
g = acceleration of gravity
h = altitude
I_{yy} = pitching moment of inertia
J = cost function, continuous time
$\hat{J}$ = cost function, discrete time
$\tilde{J}$ = cost function, augmented
k = discrete time (range) index
$L(\ )$ = cost integrand, continuous time
$\hat{L}(\ )$ = cost integrand, discrete time
L_{jj} = soft constraint coefficient
m = aircraft mass
N = discrete terminal time (range)
P = propeller power
$P_{jj}, P_{y_{jj}}$ = terminal cost coefficients
PL_{jj} = soft constraint coefficient
q = pitch rate
$\bar{q}$ = dynamic pressure $= \frac{1}{2}\rho V_a^2$
$Q_{jj}, Q_{y_{jj}}$ = cost integrand coefficients
r = range
R_{jj} = cost integrand coefficient
S = wing reference area
t = time
T = thrust
$\boldsymbol{u}$ = control vector $= (\delta E, \delta T)^T$
V = speed
$V(\ )$ = terminal cost
w_h = headwind speed
w_v = downdraft speed
$\boldsymbol{x}$ = state vector $= (V_i, \gamma_i, q_i, \alpha_i, h, r, T, \text{ or } P)^T$
α = angle of attack
δE = elevator angle
δT = throttle setting
Δ = prefix signifying perturbation from nominal
γ = flight path angle
ρ = air density
τ_e = engine response time constant

Subscripts

a = air relative
f = final value
i = inertial
k = at discrete time k
0 = nominal, trim value or initial value

Superscript

$(\dot{\ })$ = time derivative

Introduction

AIRCRAFT regularly fly in strong, steady winds without incident. They are able to do so because the winds are relatively invariant with respect to position and time, and the aircraft's air-relative velocity vector, which gives rise to the forces that support the aircraft, behaves in a predictable way that can be controlled readily by the pilot. Furthermore, high winds are encountered most often at altitude, where flight path deviations do not pose an immediate danger of ground impact. When strong winds are variable and when they are encountered near the ground (as during climb-out and approach), there is a heightened risk that the wind will cause hazardous flight path deviations.

This risk is especially pronounced for aircraft flying through *microbursts*, which are severe downdrafts accompanied by intense outflows.[1-3] In the classic example, first described by Fujita,[4] a large volume of cold air descends in a narrow column (less than 3 miles wide) that spreads out upon hitting the ground. The result is a localized region of high winds that change directions and magnitudes over short distances and short periods of time (Fig. 1). Aircraft flying through such regions are likely to be driven far from their intended paths unless proper corrective actions are taken.[5]

The archetypal microburst encounter confronts the pilot with a difficult flight path management problem, and it may be necessary for the pilot to apply counterintuitive control inputs for safe passage.[6] The aircraft flies into the outflow, experiencing a headwind increase that causes ballooning above the flight path. The pilot may be inclined to throttle back, but just as this maneuver is completed, the headwind vanishes, to

Received Aug. 13, 1985; presented as Paper 85-1833 at the 12th AIAA Atmospheric Flight Mechanics Conference, Snowmass, CO, Aug. 19-21, 1985; revision received Feb. 26, 1986.

*Graduate Student, Mechanical and Aerospace Engineering.
†Professor, Mechanical and Aerospace Engineering. Associate Fellow AIAA.

be replaced by a downdraft that is quickly followed by a tailwind. The downdraft lowers the steady-state flight path angle, and the tailwind lowers airspeed, decreasing lift. Both effects increase the descent rate. Even if the pilot takes no adverse action, the flight path excursion can be large, as shown for a typical three-engine jet transport (see Fig. 1). In the example, the wind disturbance excites the aircraft's lightly damped phugoid mode of motion, further complicating the problem of flight path control.

Having the performance capacity to fly through the microburst is not in itself sufficient to ensure a safe transit; it also is necessary to apply the right *control strategy*. Postaccident investigation of the 1982 crash of Pan American Flight 759 near New Orleans indicated that the Boeing 727 aircraft had enough power to fly through the microburst that it encountered,[1] but the pilot did not have an effective control strategy for survival. Although the best way to deal with microbursts is to avoid them, currently operational microburst detection capability may not make this possible[7]; therefore techniques for safe penetration should be understood.

Prior research indicates that realizable control strategies can do much to further this goal.[8] Related work falls in two categories: performance evaluation of existing aircraft-control system combinations[5,9,10] and piloting technique-control system modifications for improved microburst rejection.[6,11,12] In addition, work on automatic landing systems has led to systems with reduced sensitivity to wind inputs.[13] These studies have used computer simulation for evaluation and linear theory for control design.

The current study is similar to the others in its use of computer simulation and its goal of improving microburst tolerance through the application of controls; however, it is fundamentally different in its specification of control histories via numerical optimization. Rather than designing or simulating closed-loop control laws, this study has generated optimal trajectories through given wind profiles. These trajectories are physically realizable in that the wind disturbances and control inputs combine to produce the resulting flight paths, but the computation of control histories depends on prior knowledge of the wind profiles. Consequently, the objective of this paper is to show the true physical limits of the aircraft in an ideal situation, providing examples of optimal trajectories with which implementable closed-loop control laws can be compared. To this end, computational results are presented for aircraft of both the jet transport and the propeller-driven general aviation class. Wind profiles include the engineering approximation used in an earlier paper[6] and profiles drawn from Doppler radar measurements in the Joint Airport Weather Studies (JAWS) program.[14]

Analysis Highlights

Aircraft Models and Equations of Motion

Mathematical models of the aircraft are needed for flight path simulation and numerical optimization. The two models used here, a three-engine, 150,000-lb jet transport (JT) and a single-engine, propeller-driven general aviation aircraft (GA), are taken from Ref. 6. Each model consists of a system of seven ordinary differential equations, six of which describe the aircraft's longitudinal motions in a wind shear under the point-mass and quasisteady-aerodynamic assumptions.

$$\dot{V}_i = \{ -\bar{q}S[C_D\cos(\alpha_i-\alpha_a) + C_L\sin(\alpha_i-\alpha_a)] + T\cos\alpha_i\}/m - g\sin\gamma_i \tag{1}$$

$$\dot{\gamma}_i = (\{\bar{q}S[C_L\cos(\alpha_i-\alpha_a) - C_D\sin(\alpha_i-\alpha_a)] + T\sin\alpha_i\}/(m - g\cos\gamma_i)/V_i \tag{2}$$

$$\dot{q}_i = \bar{q}S\bar{c}C_M/I_{yy} \tag{3}$$

$$\dot{\alpha}_i = q_i - \dot{\gamma}_i \tag{4}$$

$$\dot{h} = V_i\sin\gamma_i \tag{5}$$

$$\dot{r} = V_i\cos\gamma_i \tag{6}$$

where

$$\alpha_a = \alpha_i + \gamma_i - \tan^{-1}[(V_i\sin\gamma_i + w_v)/(V_i\cos\gamma_i + w_h)] \tag{7}$$

$$V_a^2 = V_i^2 + w_v^2 + w_h^2 + 2V_i(w_v\sin\gamma_i + w_h\cos\gamma_i) \tag{8}$$

The seventh differential equation models a first-order lag in the engine response:

Jet transport thrust model

$$\dot{T} = (\delta T - T)/\tau_e \tag{9}$$

General aviation thrust model

$$\dot{P} = (\delta T - P)/\tau_e \tag{10}$$

$$T = E(V_a)P/V_a \tag{11}$$

Symbolically, these equations may be represented in the form: $\dot{\boldsymbol{x}} = \boldsymbol{f}(\boldsymbol{x},\boldsymbol{u},t)$, with state vector $\boldsymbol{x}$ and control vector $\boldsymbol{u}$. They incorporate the effects of two control inputs, the elevator and the throttle. They were solved using a sixth-order Runge-Kutta algorithm,[15] which was found to provide a minimum number of function evaluations per unit of simulated time.

Because there is a monotonic relationship between range and time for these flight paths and because none of the microburst models depend explicitly on time, the equations were simplified by redefining the independent variable to be the range. Equations (1-5) were divided by Eq. (6) to get dx/dr instead of dx/dt. The number of differential equations was thereby reduced, as was the amount of computation required for trajectory optimization.

There were problems encountered in optimizing the GA flight paths. The aircraft's quick short-period response combined with its low airspeed to produce an excessive number of time steps per run. As a solution, a reduced-order GA model was developed. It replaced the short-period dynamics with a quasisteady approximation through the method of residualization (or zeroth-order singular perturbation). In this approach, the differential equations Eqs. (3) and (4) are replaced by the following algebraic equations:

$$0 = \dot{q}_i = \bar{q}S\bar{c}C_M/I_{yy} \tag{12}$$

$$0 = \dot{\alpha}_a = q_i - \frac{\bar{q}SC_L + T\sin\alpha_a}{mV_a} + \frac{(g-\dot{w}_v)(V_i\cos\gamma_i + w_h) + \dot{w}_h(V_i\sin\gamma_i + w_v)}{V_a^2} \tag{13}$$

The advantage this yielded was a much faster optimization, partly because Runge-Kutta integration steps could be sized on the time scale of the phugoid period, and partly because the number of differential equations was reduced to five. The heuristic justification for this approximation goes as follows: Glide path must be maintained during a microburst encounter on either climb-out or approach, and it is hardly affected by short-period transients. Optimal control time histories derived using this model were tested in the full-order GA model through the same microburst to verify their "optimality," and differences in flight path were found to be negligible. This approximate model made optimization of GA trajectories possible on a practical basis.

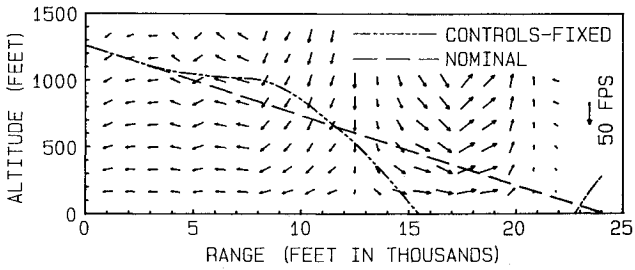

Fig. 1 Nominal and controls-fixed approach trajectories through a Joint Airport Weather Studies microburst.

Microburst Description

The equations of motion contain wind input terms. To incorporate a microburst model in them, the vertical and horizontal wind velocities were needed as functions of range, altitude, and/or time. Simplified models which contain the main features of a microburst have been used in the past.[6,10] Recently, models have become available which can simulate wind fields measured by the JAWS Doppler radar system.[5,16] For purposes of comparison, the idealized microburst of Ref. 6 was used; this is a range-dependent (1 – cos) downdraft pulse superimposed on one period of a headwind/tailwind sine-wave shear. Four JAWS microburst cross sections also were considered. Each derived vertical and horizontal winds from two-dimensional range- and altitude-dependent data tables. None of the models included wind variations at higher-frequency, turbulent scales of motion. Such an omission is reasonable because position response to high-frequency wind inputs is low.[6] These five models provided sufficient variety for a fruitful study of the microburst encounter problem via simulation and deterministic optimization.

Nonlinear Optimal Control

Optimal trajectories are calculated by finding the control history that minimizes a cost function. For the unconstrained, fixed-time, free-endpoint problem, a scalar, positive definite cost function

$$J=\int_{t_0}^{t_f} L(\boldsymbol{x},\boldsymbol{u},t)\,\mathrm{d}t + V[\boldsymbol{x}(t_f)] \tag{14}$$

is minimized by the choice of control $\boldsymbol{u}(t)$ in $[t_0,t_f]$ subject to the dynamic constraint

$$\dot{\boldsymbol{x}}=\boldsymbol{f}(\boldsymbol{x},\boldsymbol{u},t) \tag{15}$$

$$\boldsymbol{x}(t_0)=\boldsymbol{x}_0 \tag{16}$$

The specific cost functions used in this study took the general form

$$\begin{aligned} L(\boldsymbol{x},\boldsymbol{u},t) &= Q_{11}\Delta V_i^2 + Q_{22}\Delta\gamma_i^2 + Q_{33}\Delta q_i^2 + Q_{44}\Delta\alpha_i^2 \\ &+ Q_{55}[(h-h_0)\cos\gamma_{i_0} - (r-r_0)\sin\gamma_{i_0}]^2 + Q_{y_{11}}\Delta\alpha_a^2 \\ &+ Q_{y_{22}}\Delta V_a^2 + R_{11}\Delta\delta E^2 + R_{22}\Delta\delta T^2 + \delta E_{\lim}(\delta E) \\ &+ \delta T_{\lim}(\delta T) + \alpha_{\lim}(\alpha_a) + V_{\lim}(V_a) \end{aligned} \tag{17}$$

$$\begin{aligned} V(\boldsymbol{x}) &= P_{11}\Delta V_i^2 + P_{22}\Delta\gamma_i^2 + P_{33}\Delta q_i^2 + P_{44}\Delta\alpha_i^2 \\ &+ P_{55}[(h-h_0)\cos\gamma_{i_0} - (r-r_0)\sin\gamma_{i_0}]^2 + P_{y_{11}}\Delta\alpha_a^2 \\ &+ P_{y_{22}}\Delta V_a^2 + \alpha_{p\lim}(\alpha_a) + V_{p\lim}(V_a) \end{aligned} \tag{18}$$

The cost function quantifies the "goodness" of a trajectory, making it possible to compare trajectories and find the "best" one. In $L(\ )$ and $V(\ )$, the squares of the deviations from the nominal state and control time histories are weighted. Therefore, the optimal trajectory is that which minimizes the weighted mean-squared deviation from the nominal trajectory.

The incremental cost functions $\delta E_{\lim}$ and $\delta T_{\lim}$ were added as so-called soft constraints to keep control deflections within saturation limits. Similarly, $\alpha_{\lim}$, $V_{\lim}$, $\alpha_{p\lim}$, and $V_{p\lim}$ were added as soft constraints to prevent aircraft stall. Each of these functions remains zero as long as their respective arguments remain within certain limits. When the limits are violated, the contribution to the cost grows quadratically with the magnitude of the violation; for example,

$$\delta E_{\lim}(\delta E) = \begin{cases} L_{11}(\delta E-\delta E_{\min})^2 & \text{if } \delta E<\delta E_{\min} \\ 0 & \text{if } \delta E_{\min}\le\delta E\le\delta E_{\max} \\ L_{11}(\delta E-\delta E_{\max})^2 & \text{if } \delta E_{\max}<\delta E \end{cases} \tag{19}$$

The minima and maxima were chosen conservatively to ensure that the optimal trajectory would not violate the actual limits. The coefficient L_{11} is a parameter of the $\delta E_{\lim}$ cost function. Each of the soft constraint functions has one such coefficient. The correspondence between the remaining constraint functions and their associated coefficients is as follows:

Function	Coefficient
$\delta T_{\lim}(\delta T)$	L_{22}
$\alpha_{\lim}(\alpha_a)$	L_{33}
$V_{\lim}(V_a)$	L_{44}
$\alpha_{p\lim}(\alpha_a)$	PL_{33}
$V_{p\lim}(V_a)$	PL_{44}

(20)

To characterize any specific cost function of the preceding form [Eqs. (17-20)], all that must be specified are the coefficients. The nominal (glide path optimizing) coefficients were chosen to weight altitude deviations most heavily, thus minimizing the mean-squared altitude deviation:

Q_{11}	$=0/\text{ft-(ft/s)}^2$	P_{33}	$=1000/\text{(deg/s)}^2$
Q_{22}	$=4/\text{ft-deg}^2$	P_{44}	$=0/\text{deg}^2$
Q_{33}	$=4/\text{ft-(deg/s)}^2$	P_{55}	$=5000/\text{ft}^2$
Q_{44}	$=0/\text{ft-deg}^2$	$P_{y_{11}}$	$=1000/\text{deg}^2$
Q_{55}	$=20/\text{ft-ft}^2$	$P_{y_{22}}$	$=1000/\text{(ft/s)}^2$
$Q_{y_{11}}$	$=4/\text{ft-deg}^2$	L_{11}	$=190/\text{ft-deg}^2$
$Q_{y_{22}}$	$=4/\text{ft-(ft/s)}^2$	L_{22}	$=20/\text{ft-percent}^2$
R_{11}	$=40/\text{ft-deg}^2$	L_{33}	$=20/\text{ft-deg}^2$
R_{22}	$=4/\text{ft-percent}^2$	L_{44}	$=0/\text{ft-(ft/s)}^2$
P_{11}	$=0/\text{(ft/s)}^2$	PL_{33}	$=5000/\text{deg}^2$
P_{22}	$=1000/\text{deg}^2$	PL_{44}	$=0/\text{(ft/s)}^2$

(21)

This continuous-time (range) optimal control problem was transformed to a discrete-time optimal control problem for solution. A zeroth-order hold assumption was made for the control time history, and, with the help of a numerical integration scheme, the transformation was made as follows:

$$\hat{\boldsymbol{f}}[(\boldsymbol{x}_k,\boldsymbol{u}_k,k]=\boldsymbol{x}(t_{k+1}) \tag{22}$$

$$\hat{L}[\boldsymbol{x}_k,\boldsymbol{u}_k,k]=\int_{t_k}^{t_{k+1}} L[\boldsymbol{x}(t),\boldsymbol{u}_k,t]\,\mathrm{d}t \tag{23}$$

where

$$t_k=t_0+(t_f-t_0)(k-1)/(N-1) \tag{24}$$

and $\boldsymbol{x}(t)$ is a solution of the initial value problem,

$$\dot{\boldsymbol{x}}(t)=\boldsymbol{f}[\boldsymbol{x}(t),\boldsymbol{u}_k,t] \tag{25}$$

Table 1 Trajectory optimizations

Aircraft	Flight phase	Microbursts	Primary control objective
JT	Approach ($\gamma_i = -3$ deg)	All five	Glide path
JT	Climb-out ($\gamma_i = +3$ deg)	All five	Glide path
JT	Approach ($\gamma_i = -3$ deg)	Most severe JAWS headwind/tailwind shear	Glide path and airspeed
JT	Approach ($\gamma_i = -3$ deg)	Most severe JAWS headwind/tailwind shear	Airspeed
GA	Approach ($\gamma_i = -3$ deg)	Idealized plus one JAWS microburst	Glide path
GA	Climb-out ($\gamma_i = +3$ deg)	One JAWS microburst	Glide path

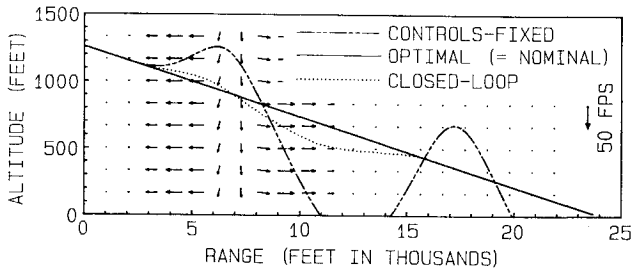

Fig. 2 Three JT approach trajectories through the idealized microburst.

$$x(t_k) = x_k \tag{26}$$

The equivalent discrete-time optimal control problem is

$$\text{find } u_k \text{ for } k = 1,\ldots,N-1 \tag{27}$$

to minimize

$$\hat{J} = \sum_{k=1}^{N-1} \hat{L}[x_k, u_k, k] + V[x_N] \tag{28}$$

subject to

$$x_{k+1} = \hat{f}[x_k, u_k, k] \tag{29}$$

$$x_1 = x_0 \tag{30}$$

The problem takes the general form of a static, finite-dimensional constrained optimization, which can be solved using functional minimization techniques. Two such techniques are 1) the steepest-descent algorithm, a first-order gradient method, and 2) Newton's second-order gradient method.[17] The *steepest-descent method* uses an initial guess for the control time history. Next it differentiates an augmented cost function $\tilde{J}$ with respect to the control time history to determine an optimization step that will yield the largest decrease in the cost. Relatively little computation is required per improvement in the control time history, but convergence properties near the optimum are poor. *Newton's method* is a generalization of the Newton-Raphson method for determination of a root of a scalar equation. In this case it is applied to the set of simultaneous equations which comprise the necessary condition for optimality: $d\tilde{J}/du_k = 0$ for $k = 1,\ldots,N-1$. It too starts with an initial guess of the control time history and makes improvements.

Newton's method requires the inversion of the matrix $d^2\tilde{J}/du_k du_i$. This matrix is large for long discrete-time histories. Its inversion could present a problem, but the special nature of the cost function and of the constraints facilitates this inversion. Although computationally more complex than the steepest-descent method, Newton's method has excellent convergence properties near the optimum. An algorithm was developed using each of these methods to advantage to solve for the control vector's optimal discrete-time history.

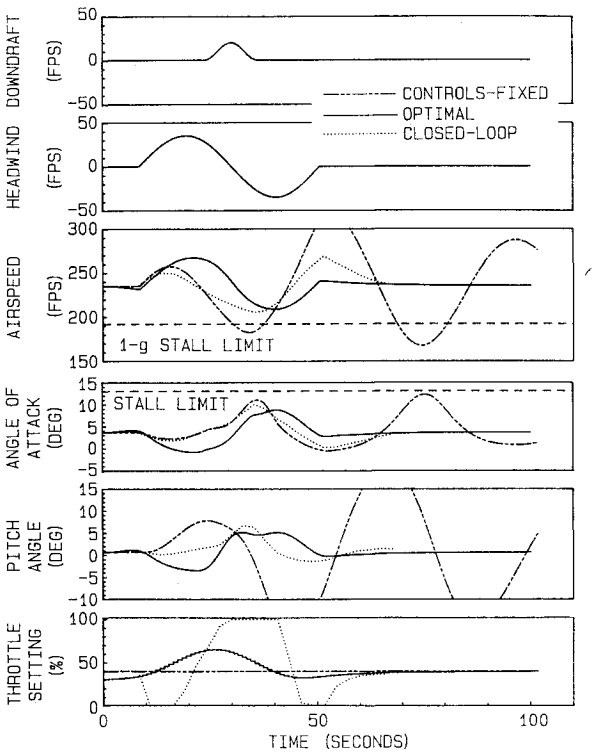

Fig. 3 Time histories associated with the JT approach through the idealized microburst.

Trajectory Optimization Results

Fifteen optimal trajectories have been computed to date (Table 1). Six of these have been selected for discussion here: 1) a glide-path-optimal JT approach trajectory through the idealized microburst, 2) a glide-path-optimal JT approach trajectory through the most severe JAWS headwind/tailwind shear, 3) a glide-path-plus-airspeed-optimal JT approach trajectory through the most severe JAWS headwind/tailwind shear, 4) an airspeed-optimal JT approach trajectory through the most severe JAWS headwind/tailwind shear, 5) a glide-path optimal GA approach trajectory through a moderate-to-severe JAWS microburst, and 6) a glide-path-optimal JT climb-out trajectory through a severe JAWS microburst.

In addition to altitude-vs-range trajectories, associated time histories will be reviewed. Vertical and horizontal wind velocities, airspeed, angle of attack, pitch angle, and throttle setting will be considered. These will provide insight as to how the optimal performance was achieved. The ultimate goal is practical application of these results to improved piloting techniques in microbursts.

Case 1: JT Approach Through the Idealized Microburst

The result for this glide-path-optimal trajectory (approximately nominal cost function) is compared with the controls-fixed case and with the best closed-loop case presented in Ref. 6. The performance of the optimal trajectory was excellent: It stayed within 2 ft of the nominal glide path. The maximum excursions from nominal of the nonoptimal closed-loop and controls-fixed cases were 180 and 1000 ft, respectively (Fig. 2). Neither of these cases came near the optimal glide-path-holding performance. Consideration of associated time histories can help explain this (Fig. 3).

The two time histories which best account for the optimal glide path performance are those of the airspeed and the angle of attack. The optimal angle-of-attack time history is just out of phase with the optimal airspeed time history. Their magnitude ratio is just right to maintain constant lift. Thus the optimal control is the opposite of standard piloting techniques. Instead of the angle of attack being used to maintain constant airspeed, it is used to maintain constant lift in the face of changing airspeed.

The optimum airspeed variation is approximately that of the microburst's horizontal wind. For this glide-path-optimal case, little control effort is expended in maintaining airspeed. This presents no problem, because the airspeed never falls below the 1-g stall limit.

The pitch-angle time history, an indication of the pilot's commands, varies considerably among the three cases. In the controls-fixed and closed-loop cases, the pitch angle is not driven low enough during the headwind zone to prevent ballooning above the glide slope. In the downdraft and tailwind zones it is not held high for enough time to keep the aircraft from falling below the intended flight path. The optimal pitch-angle time history reflects the optimal angle-of-attack time history, taking into account the changing relationship between the two angles caused by variable winds.

The use of throttle in the optimal case is greatly reduced compared to the closed-loop case, despite improved glide path performance. Its lead compared to the closed-loop setting may partially explain this.

The optimal time histories exhibit perturbations from the nominal trajectory case prior to the encounter of the microburst wind variations. This is due to the nature of the deterministic optimization; the algorithm "knows" ahead of time what is about to happen and acts accordingly. This fact precludes the implementation of this algorithm as a control law unless systems can be developed which estimate the wind ahead of the aircraft.

Case 2: JT Approach Through the Most Severe JAWS Headwind/Tailwind Shear

This trajectory demonstrates the optimal performance (nominal cost function) for the most extreme headwind/tailwind shear contained in the corridor data sets of Ref. 14. The magnitude of the shear is 85 ft/s (50 knots), and it occurs in a range spanning only 7500 ft. It corresponds to path *YZ* through the microburst that occurred on August 5, 1982 (see Ref. 5). Again, glide path is held very closely—it is indistinguishable from the nominal glide path—whereas the deviations for the controls-fixed case are on the order of 1000 ft (Fig. 4).

The airspeed, angle-of-attack, and other time histories provide the key to achieving this performance. As in the idealized microburst case, angle of attack and airspeed are just out of phase, and their magnitude ratio is sized such that the aerodynamic lift is held approximately constant (Fig. 5). For the second time, glide-path-optimal control yields unconventional pitch-angle steering in the face of varying airspeed.

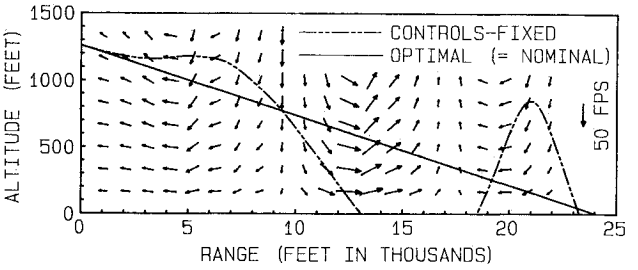

Fig. 4 Two JT approach trajectories through the most severe JAWS headwind/tailwind shear.

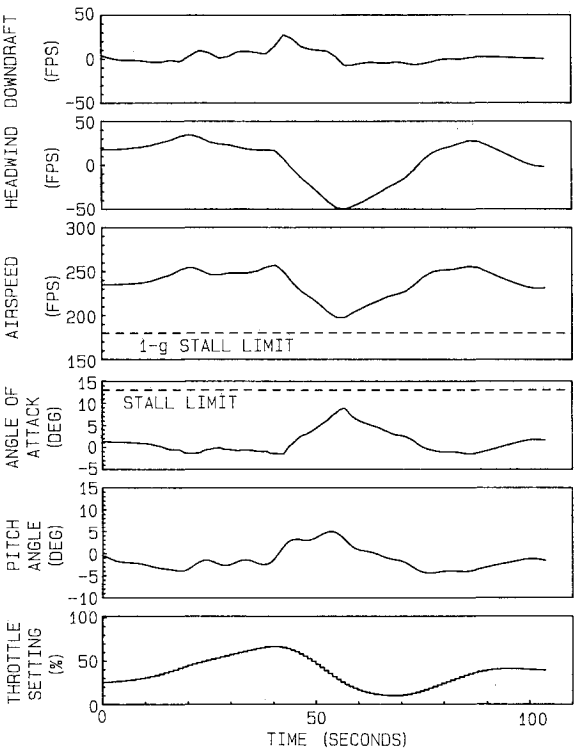

Fig. 5 Time histories associated with the optimal JT approach through the most severe JAWS headwind/tailwind shear.

Also noteworthy among these time histories are some departures from the idealized microburst pattern. First, the airspeed variations do not closely reflect those of the microburst's horizontal winds as they did in the idealized microburst case. This glide-path-optimal control is more concerned with airspeed variations. The observation helps explain a second difference: increased throttle activity. The optimal control reduces airspeed variations via throttle inputs while holding altitude via pitch steering.

One explanation for the airspeed control is that airspeed variations were moderately weighted in the cost function. On further consideration, it can be seen that some airspeed control was necessary just to maintain glide path: The total headwind/tailwind shear was large enough to cause airspeed to fall below the 1-g stall limit if left uncontrolled.

There is some doubt as to whether the optimum could be practically achieved in this case. The peak throttle setting occurs 20 s prior to the maximum tailwind. Obviously, the deterministic optimization used its foreknowledge of the wind field to advantage here. Such a strategy will become practical only when winds can be measured 1 mile ahead of the aircraft. This

wind field probably should remain classified as severe,[5] despite the excellent performance of the optimal trajectory.

Cases 3 and 4: The JT Approach Airspeed vs Glide Path as an Objective

This comparison was motivated by the common practice among pilots of maintaining airspeed via elevator inputs. Its intent is to clarify the differences between this strategy and the unconventional strategy suggested by glide-path-optimal trajectories. The conventional strategy was carried to its logical conclusion via trajectory optimization with airspeed deviations weighted most heavily in the cost function (airspeed optimal). Thus airspeed deviations would be minimized. The cost function used was identical to the nominal cost function with the following exceptions:

$$\begin{aligned} Q_{22} &= 0.004/\text{ft-deg}^2 & P_{22} &= 1/\text{deg}^2 \\ Q_{55} &= 0.02/\text{ft-ft}^2 & P_{55} &= 5/\text{ft}^2 \\ Q_{y_{22}} &= 40/\text{ft-(ft/s)}^2 & P_{y_{22}} &= 10{,}000/(\text{ft/s})^2 \end{aligned} \quad (31)$$

An intermediate result also was obtained in which both airspeed and glide path deviations had significant weightings in the cost function (glide path plus airspeed optimal). This cost function also had several differences from the nominal:

$$\begin{aligned} Q_{22} &= 0.4/\text{ft-deg}^2 & P_{22} &= 100/\text{deg}^2 \\ Q_{55} &= 2/\text{ft-ft}^2 & P_{55} &= 500/\text{ft}^2 \\ Q_{y_{22}} &= 40/\text{ft-(ft/s)}^2 & P_{y_{22}} &= 10{,}000/(\text{ft/s})^2 \end{aligned} \quad (32)$$

Neither case exhibited the trajectory tracking performance of the glide-path-optimal case. The airspeed-optimal trajectory had altitude excursions of 500 ft. The glide-path-plus-airspeed-optimal trajectory did much better (Fig. 6).

Examination of the airspeed time histories shows the other side of the coin. The airspeed-optimal case did a good job of maintaining airspeed, whereas the glide-path-optimal case did poorly on this point. The glide-path-plus-airspeed-optimal case did moderately well (Fig. 7). These results were to be expected for the given cost functions.

This is all very comforting for the fellow who wrote the optimization procedure, but what does it mean for the pilot or for the autopilot designer? The pitch-angle and throttle-setting time histories help answer this question. Throttle activity for the airspeed-optimal case was low, but pitch-angle control was pronounced. So airspeed was maintained via pitch control in the conventional manner. The glide-path-plus-airspeed case was different. Throttle activity here was extreme. Pitch control was more like the unconventional, lift-maintaining, glide-path-optimal case (see Fig. 7). The lesson to be learned was that tight airspeed control can be achieved only via pitch control at the expense of glide path control or via large throttle inputs. The former is unacceptable for terminal area flight. The latter places unreasonable demands on the engines.

Case 5: GA Approach Through a Moderate to Severe JAWS Microburst

The microburst penetration performance of the full-order GA model is demonstrated here. Its trajectory follows path *KL* through the JAWS microburst that occurred on August 5, 1982 (see Ref. 5). The control time history corresponds to the glide-path-optimal trajectory for the reduced-order GA model. The cost function is again similar to the nominal, with several exceptions:

$$\begin{aligned} Q_{22} &= 80/\text{ft-deg}^2 & P_{y_{22}} &= 1000/(\text{ft/s})^2 \\ Q_{33} &= 80/\text{ft-(deg/s)}^2 & L_{33} &= 200/\text{ft-deg}^2 \\ P_{22} &= 20{,}000/\text{deg}^2 & PL_{33} &= 0/\text{deg}^2 \\ P_{33} &= 0/(\text{deg/s})^2 & PL_{44} &= 3000/(\text{ft/s})^2 \\ P_{y_{11}} &= 0/\text{deg}^2 \end{aligned} \quad (33)$$

Glide path error is held within 30 ft for the optimal case, as opposed to 1000 ft and over for the controls-fixed case (Fig. 8). Although this tracking performance is quite good, the reduced-order optimization indicated even better results. Lag in the angle-of-attack response to elevator inputs accounts for this discrepancy. The full-order model does not respond as quickly to elevator commands as the reduced-order model expects, so the angle of attack, and hence the lift, is not exactly what the reduced-order optimization expects.

As for the associated time histories (Fig. 9), they are similar to those of case 2, the JT trajectory through the most severe JAWS headwind/tailwind shear. The angle of attack is out of phase with the airspeed so as to keep lift constant. Strong throttle activity anticipates and averts a windshear-induced airspeed excursion below the 1-*g* stall limit. It is important to note that this weaker microburst presents as much difficulty for the GA aircraft as did the stronger one for the JT aircraft.

Another interesting feature of these plots is the correlation between fluctuations in the throttle setting and fluctuations in the downdraft velocity. The GA aircraft has a limited ascent rate capability. In order to maintain its glide path, it demands appreciable throttle adjustments whenever it encounters a downdraft.

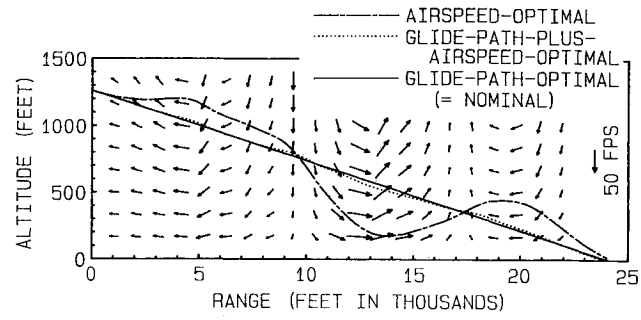

Fig. 6 Three JT approach trajectories through the most severe JAWS headwind/tailwind shear.

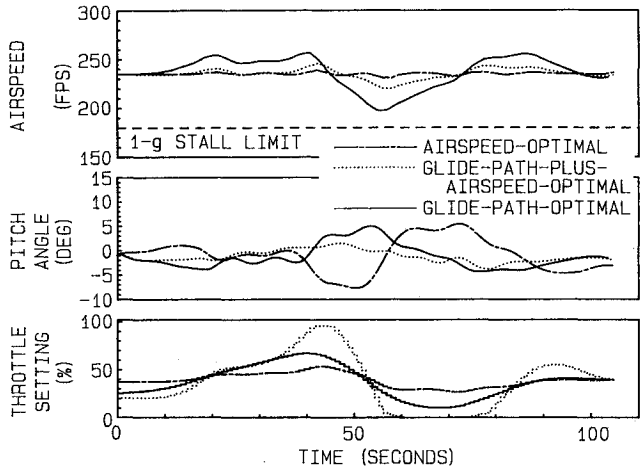

Fig. 7 Airspeed vs glide path objectives: time histories associated with the JT approach through the most severe JAWS headwind/tailwind shear.

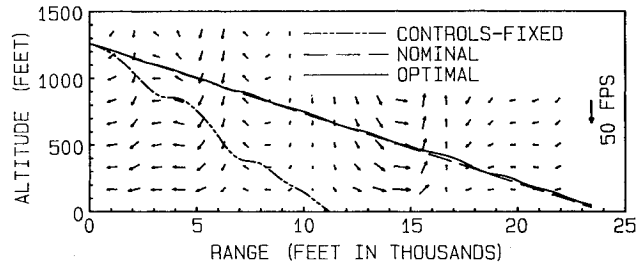

Fig. 8 Three GA approach trajectories through a JAWS microburst.

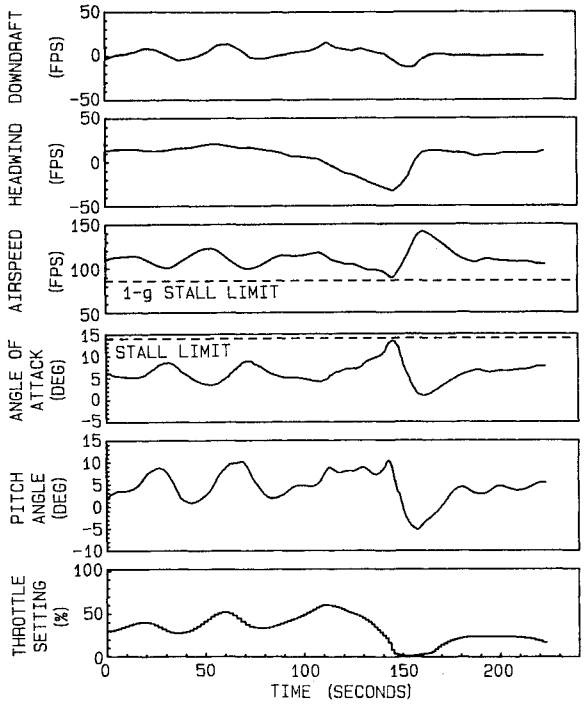

Fig. 9 Time histories associated with the optimal GA approach through a JAWS microburst.

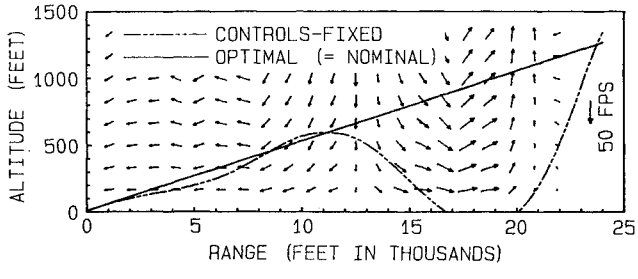

Fig. 10 Two JT climb-out trajectories through a JAWS microburst.

Case 6: JT Climb-Out Through a Severe JAWS Microburst

Glide-path-optimal climb-out trajectory performance is demonstrated by this example. The nominal cost function applies here. The flight path follows line *AB* through the microburst of August 5, 1982 (see Ref. 5). This particular wind field cross section was chosen because it represents the shortest length scale of all JAWS microburst corridors available in Ref. 14, coming nearest to excitation of the JT at its phugoid natural frequency. As in the previous glide-path-optimal JT cases, trajectory tracking performance is exceptional (Fig. 10).

The associated time histories, although not shown, demonstrate control procedures similar to those of case 2: A pitch-up response to airspeed loss is used to maintain lift, and throttle control is used to avert stall by anticipating extreme losses of relative headwind. Throttle saturation occurs in this case because of the high nominal takeoff setting. Fortunately, airspeed did not fall below the 1-*g* stall limit, so flight path deviations could be kept to a minimum via pitch steering.

Conclusions

Throughout this study a recurrent theme was found: The nonlinear, deterministic flight-path-optimal trajectories displayed excellent flight path tracking performance. This was true for both the GA and JT aircraft models in all microbursts considered. Physical limits such as maximum thrust and stall angle of attack were not appreciably exceeded to accomplish this. Therefore the aircraft were physically able to penetrate these microbursts safely. Some of these wind fields have been classified as severe.[5] Thus an aircraft's ability to penetrate a microburst safely may depend more upon control law design limits than upon airframe or engine performance limits.

The other major theme found in the case studies involved the issue of desired outputs and available control inputs. The two desired outputs were altitude and airspeed. The two available inputs were throttle setting and elevator angle (or pitch control). Pitch control was found to be an effective input on the time scale of a microburst encounter, capable of maintaining constant airspeed or nominal flight path, but not both. Throttle setting, while not as effective in this situation, proved helpful in severe microbursts. In these cases the aircraft would have stalled without it, had they been attempting to hold flight path. Optimal trajectory tracking was seen to use pitch control in an unconventional manner to maintain lift while loosely controlling airspeed via throttle inputs.

These computational results reveal new perspectives on the ability of two types of aircraft to fly through microbursts. Future research will indicate how practical control systems can use this information to attain a greater level of protection against the hazards of microburst encounter.

Acknowledgments

This research was supported in part by the Federal Aviation Administration and the National Aeronautics and Space Administration under Grant No. NGL 31-001-252. Mark L. Psiaki is supported by a National Science Foundation Graduate Fellowship.

References

[1]"Pan American World Airways, Inc., Clipper 759, Boeing 727-235, N4737, New Orleans International Airport, Kenner, Louisiana, July 9, 1982," National Transportation Safety Board, Washington, DC, Aircraft Accident Report-83/02, March 1983.

[2]"Aviation Weather," U.S. Congressional Hearing, Aug. 11, 1982.

[3]Townsend, J. (ed.), "Low-Altitude Wind Shear and Its Hazard to Aviation," National Research Council, Washington, DC, Sept. 1983.

[4]Fujita, T. T., "Downbursts and Microbursts—An Aviation Hazard," *Proceedings of the 19th Conference on Radar Meteorology*, American Meteorological Society, Boston, MA, 1980, pp. 94-101.

[5]Frost, W., Chang, H. P., Elmore, K. L., and McCarthy, J., "Simulated Flight Through JAWS Wind Shear," *Journal of Aircraft*, Vol. 21, Oct. 1984, pp. 797-802.

[6]Psiaki, M. L. and Stengel, R. F., "Analysis of Aircraft Control Strategies for Microburst Encounter," *Journal of Guidance, Control, and Dynamics*, Vol. 8, Sept.-Oct. 1985, pp. 553-559.

[7]McCarthy, J., "JAWS Interim Report for Third Year's Effort (FY-84) and Recent Reports from the JAWS Project," National Center for Atmospheric Research, Boulder, CO, JAWS NCAR Rept. No. 01-85, Oct. 1984.

[8]Stengel, R. F., "Solving the Pilot's Wind Shear Problem," *Aerospace America*, Vol. 23, March 1985, pp. 82-85.

[9]Frost, W. and Crosby, B., "Investigations of Simulated Aircraft Flight Through Thunderstorm Outflows," NASA CR 3052, Sept. 1978.

[10]Frost, W., "Flight in Low-Level Wind Shear," NASA CR 3678, March 1983.

[11]Lehman, J. M., Heffley, R. K., and Clement, W. F., "Simulation and Analysis of Wind Shear Hazard," Federal Aviation Administration, Washington, DC, RD-78-7, Dec. 1977.

[12]Rynaski, E. G. and Govindaraj, K. S., "Control Concepts for the Alleviation of Windshears and Gusts," NASA CR 166022, July 1982.

[13]Urnes, J. M., Hess, R. K., Moomaw, R. F., and Huff, R. W., "H-Dot Automatic Carrier Landing System for Approach Control in Turbulence," *Journal of Guidance and Control*, Vol. 4, March-April 1981, pp. 177-183.

[14]Frost, W., Chang, H. P., Elmore, K. L., and McCarthy, J., "Microburst Wind Shear Models from Joint Airport Weather Studies (JAWS)," Federal Aviation Administration, Washington, DC, PM-85-18, June 1985.

[15]Butcher, J. C., "On Runge-Kutta Processes of High Order," *Journal of the Australian Mathematical Society*, Vol. 4, Feb. 1964, pp. 179-194.

[16]Bray, R. S., "A Method for Three-Dimensional Modeling of Wind-Shear Environments for Flight Simulator Applications," NASA TM-85969, July 1984.

[17]Bryson, A. E. and Ho, Y. C., *Applied Optimal Control*, Hemisphere, New York, 1975, pp. 221-234.